Studies of a weak polyampholyte at the air–buffer interface: The effect of varying *p*H and ionic strength

Pietro Cicuta and Ian Hopkinson[a)]
Cavendish Laboratory, University of Cambridge, Cambridge CB3 0HE, United Kingdom

(Received 20 December 2000; accepted 23 February 2001)

We have carried out experiments to probe the static and dynamic interfacial properties of β-casein monolayers spread at the air–buffer interface, and analyzed these results in the context of models of weak polyampholytes. Measurements have been made systematically over a wide range of ionic strength and *p*H. In the semidilute regime of surface concentration a scaling exponent, which can be linked to the degree of chain swelling, is found. This shows that at *p*H close to the isoelectric point, the protein is compact. At *p*H away from the isoelectric *p*H the protein is extended. The transition between compact and extended states is continuous. As a function of increasing ionic strength, we observe swelling of the protein at the isoelectric *p*H but contraction of the protein at *p*H values away from it. These behaviors are typical of a those predicted theoretically for a weak polyampholyte. Dilational moduli measurements, made as a function of surface concentration exhibit maxima that are linked to the collapse of hydrophilic regions of the protein into the subphase. Based on this data we present a configuration map of the protein configuration in the monolayer. These findings are supported by strain (surface pressure) relaxation measurements and surface quasielastic light scattering measurements which suggest the existence of loops and tails in the subphase at higher surface concentrations. © *2001 American Institute of Physics.* [DOI: 10.1063/1.1365401]

I. INTRODUCTION

A polyampholyte is a polymer which contains both positively and negatively charged monomers.[1] A weak polyampholyte is one where the overall charge can be adjusted by varying external conditions, usually the *p*H. This can lead to overall neutral polyampholytes, whose net charge is zero, or polyampholytes which have a net positive or negative charge. The behavior of such molecules is of interest because amongst their number are found the proteins. An understanding of the way in which polyampholytes behave, in particular the transition from an open coil to a compact globule, may give some insight to the understanding of protein folding.

Polyampholytes are also of interest industrially. Polymers with a net charge, polyelectrolytes, are often used as stabilizers, thickeners, and in oil recovery. However, in situations of high salinity, commonly found in oil recovery, their thickening effect declines dramatically. Polyampholytes hold out the prospect of overcoming this limitation.

There have been a number of theoretical approaches to analyzing polyampholytes, these include scaling arguments,[2] Monte Carlo simulations,[3–6] molecular dynamics,[7] Flory theory models,[8] and analogies with charged droplets.[4] Previous experimental studies on polyampholytes have looked at the swelling of gels,[9–11] or the changes in viscosity of polyampholyte solutions.[11]

The study of polymers at air–liquid and liquid–liquid interfaces is of technological and academic interest.[12–14] This is a result of the importance of polymers at interfaces as stabilizers in multiphase systems and as modifiers of interfacial properties. More recently, attention has turned towards charged polymers, which introduce added complexity through electrostatic interactions. This is in part through a desire to understand the properties of natural polymers, such as proteins and polysaccharides, which are usually charged.

Close to overall neutrality, polyampholytes collapse to a compact configuration. This is because the chain can rearrange in order to facilitate attractive opposite-charge interactions which leads to a compact state. Above a net charge $eN^{1/2}$, where N is the number of monomers and e is the charge density, the chains swell. This is because, as the net charge on the polyampholyte increases, it becomes increasingly difficult to rearrange to a configuration that allows opposite charge attractions without incurring an energy penalty through the now more numerous like-charge repulsions. In three dimensional synthetic polyampholyte gels the swelling transition is abrupt. As a function of ionic strength, gels with a net charge are found to be compact at very low ionic strength, swelling to a maximum then collapsing. At very high ionic strength they swell again, this arises from the osmotic pressure of a large number of counterions condensed onto the polyampholyte. Analogies with charged liquid droplets and Monte Carlo simulations suggest that, at overall charges beyond the $eN^{1/2}$ threshold, polyampholytes will break up into a ''string of pearls,'' where the number of ''pearls'' is $\approx Q/Q_c$, where Q_c is the threshold charge described above and Q is the net charge. At high ionic strengths polyampholytes behave like polyelectrolytes through the screening of charge by counterion condensation.

Measurements of surface pressure (Π)–surface concentration (Γ) curves of interfacial layers are the two-dimensional equivalent of pressure–volume curves and in a similar manner can provide information on the inter- and

a)Electronic mail: Ian.Hopkinson@phy.cam.ac.uk

intramolecular interactions controlling the properties of the layer. At low surface concentrations molecules move independently in the so-called dilute regime. There is a surface concentration $\Gamma=\Gamma^*$ beyond which polymer molecules start to overlap, this marks the beginning of the ''semidilute'' regime. The behavior of the $\Pi-\Gamma$ isotherm in the semidilute regime of a polymer layer can be used to measure the Flory–Huggins exponent[15] which is related to the relative ''compactness'' of a polymer molecule. Measurements of interfacial strain relaxation can be made which, in common with comparable bulk measurements, can give an insight into molecular relaxations.

In this work in addition to using ''zero frequency'' interfacial techniques, we have also applied surface quasielastic light scattering (SQELS) to probe the interfacial properties at high frequency. Langevin[16] gives an excellent review of the technique and its applications. Surface quasielastic light scattering measures the power spectrum of the thermally driven fluctuations of a fluid interface, and from this information the viscoelastic properties of that interface can be determined. The measured thermally driven fluctuations typically have wavelengths of the order of 100 μm, amplitudes of the order 2 Å, and frequencies of the order 10 kHz. Here we use SQELS for two particular reasons. First, SQELS probes the interfacial properties at high frequencies compared to any other conventional method, thus it is relevant to rapid events found in processes such as emulsification. Second, we can obtain a dilational viscosity, ϵ', which is not otherwise measurable in this frequency regime. This dilational viscosity is helpful in validating models for the behavior of the surface dilational modulus with frequency.

In this work β-casein was used as a model, weak polyampholyte. β-casein is a milk protein with a random coil structure and a molecular weight of $\approx$24 kDa. It is used extensively in the food industry as an ''emulsifier.'' Its emulsifying properties are believed to arise from the blocky distribution of hydrophilic and hydrophobic residues along its length. We have calculated the likely charge distribution on the protein from the published primary sequence[17] and the known dissociation constants for amino acids. This calculation shows overall neutrality at around pH$=5$, in agreement with the published isoelectric point.[18] An overall positive net charge is found below this pH, and an overall negative charge above it. We estimate the net charge to be around -10 at pH$=9$. The total number of charges on the molecule is between 30 and 50 throughout the investigated range of pH. We observe the well known hydrophilic tail at the N-terminal, and in addition tentatively identify two further hydrophilic regions. One of these is more substantial and lies in the middle of the chain, the other lies near the C-terminal end.

Neutron reflectometry[19] and ellipsometry experiments[20,21] have been performed on β-casein at high surface coverages. They have shown that the protein adsorbs to the interface with a thin dense layer right at the surface and a thicker, less dense layer beneath it. It has been proposed that this sublayer is composed of the hydrophilic N-terminal end of the molecule. This picture is supported by proteolytic cleavage experiments[22] which show the loss of this terminal region when the adsorbed protein is exposed to a cleavage enzyme. Monte Carlo simulations[23] and self-consistent field simulations[24] have been carried out using monomer sequences which replicate β-casein on a coarse grain level. These simulations are in agreement with the experimental observations, showing a dense surface layer and a less dense sublayer corresponding to hydrophilic regions of the protein.

The experiments presented here complement these studies because they focus on a lower surface concentration, where neutron experiments have not been done. Furthermore, we have looked systematically at the behavior of β-casein on buffers of a wide range of pH and ionic strength.

Douillard[25] and Aguié-Béghin[26] have used scaling arguments to model the surface pressure–concentration isotherm of protein layers and interfacially adsorbed multiblock copolymers. These models provide a general framework which is not inconsistent with the behavior of β-casein, however they do not directly account for changes in behavior with pH and ionic strength. Fainerman and Miller[27] have made predictions of the shape of the isotherm at high Γ by considering the thermodynamics of aggregates and their equilibrium in the surface layer.

There are a number of key parameters important in the study of solutions containing charged molecules. The Bjerrum length, l_B, is the distance from a charge at which electrostatic and thermal energies are comparable,

$$l_B=\frac{e^2}{4\pi\epsilon_r\epsilon_0 k_B T}, \tag{1}$$

where e is the electron charge, ϵ_r is the relative permittivity of water, ϵ_0 is the permittivity of vacuum, k_B is the Boltzmann constant and T is the temperature. In water at room temperature the Bjerrum length is 7.14 Å. (Note that definitions in the literature appear to vary, but this is normally because factors of 4π are required in converting between CGS and SI units.) The Debye length, κ^{-1}, gives a measure of the distance at which electrostatic interactions are screened out by the presence of ions in solution,

$$\kappa^{-1}=(8\pi n l_B)^{-(1/2)}, \tag{2}$$

where, n is the number density of charges. In the NaCl solutions used here, $r_D=3.035\ \text{Å}/I^{1/2}$, where I is the molar ionic strength. In this work the Debye length varies from 96 Å at $I=0.001$ M to 3 Å at $I=1.1$ M. A final quantity of interest is the ''effective'' temperature, t. This is given by[8]

$$t=\frac{bN}{l_B(N^+ + N^-)}, \tag{3}$$

where N is the number of monomers per chain, N^+ and N^- are the numbers of positive and negative charges on the chain. b is the statistical segment length of the protein. For β-casein in guanidinium chloride (Gdn–HCl) solution the radius of gyration, Rg, measured by neutron scattering is 69 Å,[28] therefore $b=11.7$ Å [since $R_g=(N/6)^{1/2}b$]. Clearly, we would expect the radius of gyration to vary with solution conditions, we simply use these data to show that l_B and b are of the same magnitude. In these experiments (N^+

$+N^-$) lie in the range 30–50, therefore the system is always in the ''high effective temperature'' limit. In order to reach the low temperature limit it is necessary to use a very highly charged molecule.

II. EXPERIMENTAL METHODS

A. Materials

β-casein (Sigma, C-6905, 90% pure) was used as supplied. 1 mg/ml solutions in deionized water were prepared from the dried, powdered protein, stored in a refrigerator and used within 5 days. Buffer solutions were made up using deionized (Elgastat UHQ, Elga, U.K.) water. Buffers with a range of *p*H and ionic strength were prepared. For *p*H in the range 5.8–8.5 phosphate buffer was used, below *p*H=5.8 citrate buffer was used, and above *p*H=8.5 carbonate buffer.[29] To control ionic strength NaCl was added, quoted ionic strengths also include the contribution of the buffer salts. Buffer *p*H were measured using an electronic meter (ATI Orion, USA) before use.

B. Langmuir trough methods

Surface pressure vs area isotherms were measured using a Langmuir trough with a filter paper Wilhelmy plate sensor (Nima Technology, U.K.) mounted on an active antivibration table (Halycion, Germany), both of which were enclosed in a draft proof enclosure. These procedures, which reduce extraneous vibration, are necessary in order to carry out the SQELS measurements described below. The PTFE trough, area 530 cm^2 was filled with approximately 500 ml of the appropriate buffer. Surface pressure–area isotherms of the ''bare'' buffer were measured before each experiment. The surface was aspirated and the isotherm remeasured until it showed no increase in surface pressure on full compression. This was to ensure there was no surface contamination prior to the addition of the β-casein. β-casein was spread on the surface of the buffer by careful dropwise addition of the appropriate volume of the 1 mg/ml protein solution. The initial volume of added protein solution was chosen such that the surface layer was initially in the dilute regime. Typically the volume dispensed was $\approx$25 μl. Lower concentrations of spreading solution were found to lead to loss into the subphase on spreading. Repeated spreading was used to explore a greater concentration range than possible with a single compression. Since hysteresis is observed upon expansion following compression to high pressures ($\Pi > 10\times10^{-3}$ N/m), no data are presented from compressions of monolayers having such a history. These methods has been validated for β-casein in Ref. 30. The temperature of the trough was held at 22 °C by running water from a temperature controlled water bath (Haake, Germany) through channels in the base of the Langmuir trough. A header tank was used to avoid transmitting vibrations to the liquid surface.

Three types of measurement were made:

(1) Surface pressure(Π)–surface concentration(Γ) isotherms, the surface pressure was measured as the trough barrier was moved at a constant compression rate of 40 cm^2/min;

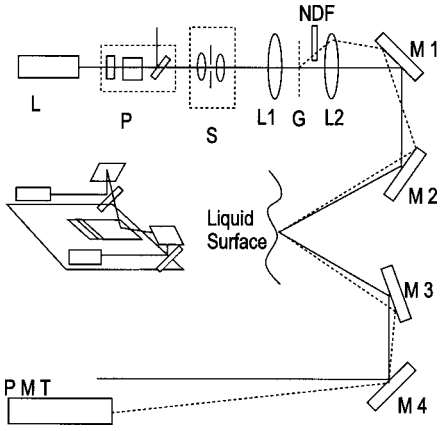

FIG. 1. Schematics of the SQELS apparatus, with inset showing an isometric view. Symbols are explained in the text.

(2) Step compression measurements, the surface area, A, was changed by a constant amount ($\Delta A/A = 0.55$) at a barrier speed of 1800 cm^2/min. The subsequent evolution of the surface pressure was measured for 15 min. The trough area was then further reduced and the next relaxation measured. Beyond this initial period we do not observe further aging effects up to a period of 3–4 h, the maximum time after spreading for which we make any measurements. We are aware that over a period of many hours and even days such aging has been observed, particularly for adsorbed monolayers;
(3) SQELS measurements were made during the relaxation phase of the step compression experiments. The magnitude of the pressure relaxation is small when compared to the accuracy of the SQELS measurement.

C. Surface quasielastic light scattering

We use a SQELS apparatus, built in house, based on a design proposed by Earnshaw[31] and Hård,[32] this is illustrated schematically in Fig. 1. The goal of such an apparatus is to measure the power spectrum of light scattered inelastically from the capillary waves at the fluid interface as a function of scattering vector, q, measured relative to the specular reflection. Photon correlation spectroscopy (PCS) is a convenient means by which to measure the small shifts in frequency that this entails. The photon correlation is done in heterodyne mode and so it is necessary to provide a coherent source of light of the original frequency at the appropriate q value. This light is provided using a weak diffraction grating. In order for the heterodyne signal to dominate the correlation function, the ratio of the intensity of the inelastically scattered light to the ''reference'' light must be adjusted to a value of the order of 10^{-3}.

Turning to Fig. 1: Light, with a wavelength of 532 nm, is provided by a 150 mW single mode diode pumped solid state laser (Laser Quantum, U.K.). Polarization and intensity are controlled using the combination of the half-wave plate ($\lambda/2$) and prism polarizer (P). The beam size, profile and collimation are controlled using the spatial filter, S. The grating (G) provides a fan of diffracted ''reference'' beams. The lenses L1 ($f=150$ mm) and L2 ($f=350$ mm) perform two tasks;

they converge the reference beams and the main beam to a single spot at the fluid interface and they focus the reference beams and the main beam in the front plane of the photomultiplier, situated ≈2 m after the surface. The relative intensity of the reference beams is adjusted by inserting a neutral density filter (NDF) so that it intercepts the diffracted spots but not the main beam. The mirrors M1–M4 direct light from the laser onto the surface and from there into the detector. The light is detected using a photomultiplier (PMT) and processed using a PC-card based photon correlator (BI9000, Brookhaven Instruments, USA), the pulse discriminator used in the PMT is modified to allow the use of the ''multiphoton'' mode originally described by Earnshaw.[33] At the detector the laser light appears as a bright central spot with a series of focused reference spots at 2–3 mm intervals away from the central spot. Each of these spots is composed of the reference beam originating from the diffraction grating and inelastically scattered light from the main beam. The reference beams are sufficiently weak that inelastic scatter from them can be ignored. Each spot corresponds to light being scattered to a different q value, the mirror M4 is adjusted in order that the appropriate reference beam falls on the detector. The value for the scattering vector, q, and the instrument resolution at a particularly reference spot was calibrated by fitting the measured correlation function for a pure liquid (water) at that point. Quoted values of the interfacial properties are the mean of values derived from fitting 5 correlation functions acquired consecutively under the same conditions, with each correlation function accumulated over two minutes. To reduce stray light, a mirror on the trough bottom deflects away from the forward direction any light that had not been specularly reflected by the buffer interface.

SQELS data were acquired from protein decorated air–buffer interfaces maintained in a Langmuir trough as described above. Data for a particular surface concentration were acquired with the barrier of the trough stationary, although we have found it possible to acquire data from a protein layer undergoing very slow compression.

D. Data analysis methods

1. Dilational moduli

The surface pressure, Π, of a protein layer is the difference between the surface energy per unit area of the bare buffer, γ_0, and the surface energy measured with the layer in place, γ. Features in the Π–Γ isotherms are seen more clearly if the dilational modulus, ϵ_{st}, is calculated from the isotherm, and this is then plotted as a function of Γ. For an insoluble layer,

$$\epsilon_{st}=\Gamma\frac{d\Pi}{d\Gamma}. \tag{4}$$

The dilational modulus is the in-plane ''dilational'' elasticity of the surface layer. For uniaxial stress, as found in the measurements made here, the dilational modulus is the sum of the compressional and shear moduli.[34]

2. Scaling exponents

The Π–Γ isotherms can be described in the semi-dilute regime using a scaling law, with exponent y,

TABLE I. Values of the two-dimensional ($\nu 2$) and three-dimensional ($\nu 3$) theoretically calculated Flory exponents, and values of the corresponding ($y2$ and $y3$) exponents y ($\Pi\propto\Gamma^y$ in the semidilute regime), for different solvent conditions.

Conditions	$\nu 2$	$\nu 3$	$y2$	$y3$
Extended chain	1	1	2	3/2
Good solvent	3/4	3/5	3	9/4
θ solvent	4/7	1/2	8	3
Poor solvent	1/2	1/3	∞	∞

$$\Pi\propto\Gamma^y. \tag{5}$$

This was introduced by Daoud, Jannik, and de Gennes,[15,35] first verified for a polymer monolayer by Vilanove[36] and has since been applied to a wide range of polymer monolayers.[12] Douillard[25] and Aguié-Béghin[26] have further developed these ideas to apply to multiblock copolymers. The Flory scaling exponent, ν, relating the chain radius of gyration, R_g, to the number of monomers, N,

$$R_g\propto N^{\nu} \tag{6}$$

is connected to y by $y=2\nu/(2\nu-1)$ in 2D, and $y=3\nu/(3\nu-1)$ in 3D. The value of the exponents are different in 2D and 3D chains, and expected values are summarized in Table I for different solvent conditions. In 2D y is small ($y=3$) for good solvents and increases to $y=8$ as solvent quality moves towards the θ conditions. Here we use the scaling exponent as a measure of the overall compactness of the protein rather than trying to link observed behavior to very specific changes. We can measure the scaling exponent from the slope of the log–log plot of Π–Γ. However, the slope of the ϵ–Π plot[26] also recovers the exponent y and this method is preferred because it is not sensitive to errors in the amount of spread solution. We find in all conditions that the ϵ–Π plot is linear in, at least, the surface pressure range $0-2\times10^{-3}$ N/m.

3. Surface quasielastic light scattering

SQELS data are normally analyzed in terms of a model treating the interfacial layer as a thin flat elastic sheet at the interface.[37] More recently Buzza *et al.*[38] have proposed a model that explicitly incorporates features of a polymer brush into the model of the interfacial layer, introducing bending and coupling moduli. Numerical analysis showed that the Buzza model would reduce to a thin viscoelastic sheet for the interfacial layer thickness measured for β-casein. We base our presentation of the key results for the analysis of SQELS data on the paper by Earnshaw *et al.*[37] and refer to the paper by Buzza *et al.*[38] for some clarification and issues related specifically to polymer monolayers. The dispersion relation $D(\omega)$ for waves at an air–liquid interface, bearing a thin viscoelastic layer, is given by

$$D(\omega)=[\epsilon q^2+i\omega\eta(q+m)]\left[\gamma q^2+i\omega\eta(q+m)-\frac{\rho\omega^2}{q}\right]-[i\omega\eta(m-q)]^2, \tag{7}$$

where m is

$$m=\sqrt{q^2+i\frac{\omega\rho}{\eta}},\quad \mathrm{Re}(m)>0, \tag{8}$$

η is the subphase viscosity, ρ is the subphase density, γ is the surface tension (or transverse modulus), and ϵ is the dilational modulus.

Solving this equation for $D(\omega)=0$ gives us an expression for the wave frequency, ω, as a function of the scattering vector q. The solutions describe both dilational and transverse waves. In a light scattering experiment it is only the transverse waves that scatter light and their power spectrum $P_q(\omega)$ is given by

$$P_q(\omega)=\frac{k_BT}{\pi\omega}\mathrm{Im}\left[\frac{i\omega\eta(m+q)+\epsilon q^2}{D(\omega)}\right]. \tag{9}$$

The behavior of the dilational waves can be inferred because of their coupling to the transverse waves. A fluid–fluid interface can be modeled using a trivial modification of Eq. (7). In the experiments carried out here a photon correlation spectrum is acquired. After accounting for instrumental factors this is simply the time Fourier transform, $P_q(t)$ of the power spectrum, $P_q(\omega)$. The dilational modulus can be expanded to take into account viscous effects,

$$\epsilon=\epsilon_0+i\omega\epsilon', \tag{10}$$

where ϵ_0 is the dilational modulus and ϵ' is the dilational viscosity. Buzza *et al.* have shown that such an expansion is not appropriate for the surface tension, and γ' should be set to zero. In this work data is analyzed by directly fitting the measured correlation function with a correlation function, $P_q(t)$, curve calculated from the interfacial properties.[37] The interfacial parameters ϵ, ϵ', and γ are all fitted simultaneously. An example of raw $P_q(t)$ correlation data fitted with a modeled function as described above is shown in Fig. 2. An alternative approach is to fit the correlation function with a damped cosine which approximates the correlation function calculated using the dispersion relation. Then either the fitted frequency and damping or values of the interfacial properties which are consistent with the values of frequency and damping can be quoted.[39] Since there are three interfacial properties and only two parameters, it is necessary, in this latter case, to make some assumptions.

III. RESULTS AND DISCUSSION

A. Surface pressure (Π)–surface concentration (Γ) isotherms

Figure 3 shows a selection of surface pressure (Π)–surface concentration (Γ) isotherms for β-casein spread on buffers at a range of *p*H values, measured using a Wilhelmy plate. The accuracy in measuring Π is 0.02×10^{-3} N/m. For a single run the random error in the surface concentration is negligible, comparing between isotherms from different runs there is a random error of around 15% in surface concentration. However, once this offset in surface concentration is corrected for, the isotherms are highly repeatable.

At low concentrations the pressure is very low, corresponding to a dilute regime of isolated proteins at the surface.[12] As the surface concentration increases the pressure starts to increase markedly, this is the point where the proteins at the surface come into contact with each other and marks the onset of the semidilute regime $\Gamma=\Gamma^*$. The behavior in this regime clearly varies with the *p*H, with the isotherm becoming flatter as the *p*H, and thus overall charge, is increased. At the highest surface concentrations the isotherms appear to converge to a universal concentrated regime, where there is significant chain overlap. We can estimate the radius of a protein molecule on the surface from the upturn concentration Γ^*. Γ ranges from 0.25×10^{-3} g/m^2 for high *p*H to 0.5×10^{-3} g/m^2 at the isoelectric *p*H. This leads to protein radiuses that increase from 51 Å at the iso-

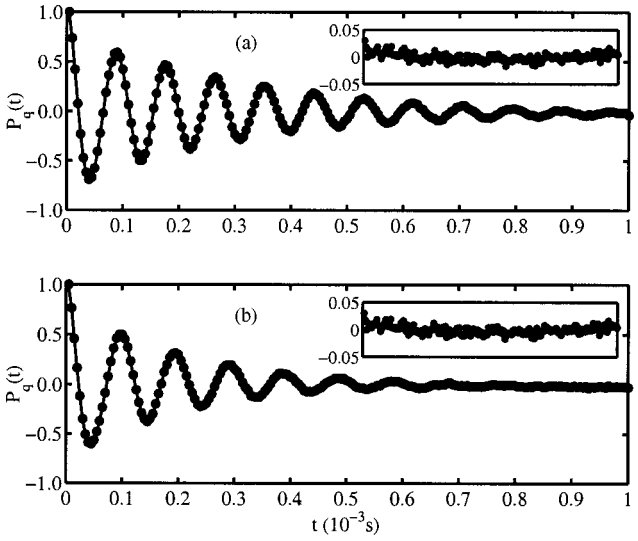

FIG. 2. Typical correlation functions obtained by surface quasielastic light scattering at subphase *p*H=5.24 and scattering vector $q=425$ cm^{-1} under different conditions (a) ''bare'' buffer; (b) β-casein monolayer at concentration $\Gamma=1\times10^{-3}$ g/m^2 and pressure $\Pi=6.3\times10^{-3}$ N/m. The solid lines are fits with the model described in the text, and insets show the residuals of the fits.

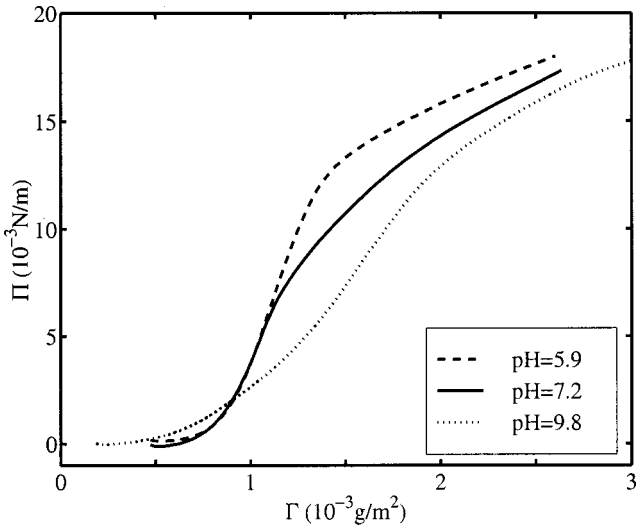

FIG. 3. Surface pressure (Π)–surface concentration (Γ) isotherms, obtained using a Wilhelmy plate, for different *p*H values, at constant ionic strength $I=0.01$ M.

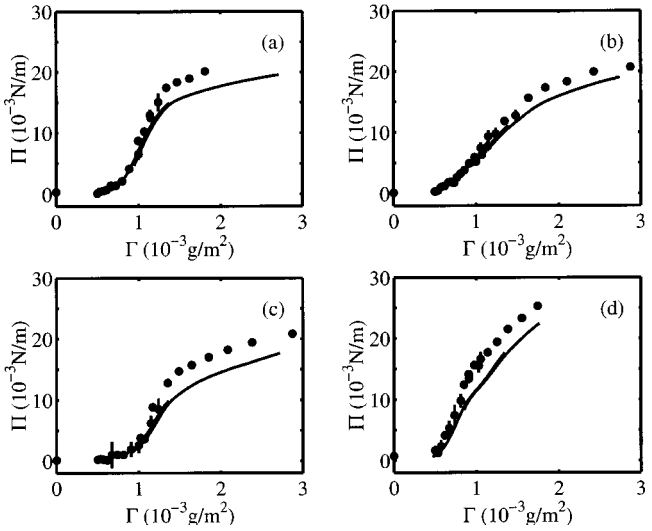

FIG. 4. Comparison of ''static'' Π–Γ isotherms (solid line) to isotherms obtained from surface light scattering for different subphase conditions (points): (a) *p*H=5.24, $I=0.01$; (b) *p*H=8.30, $I=0.01$; (c) *p*H=8.34, $I=0.001$; (d) *p*H=7.60, $I=1.1$. The scattering vectors q are in the range $425<q/\mathrm{cm}^{-1}<507$. Error bars are the standard deviation of the mean arising from the average of values obtained by fitting 5 correlation functions.

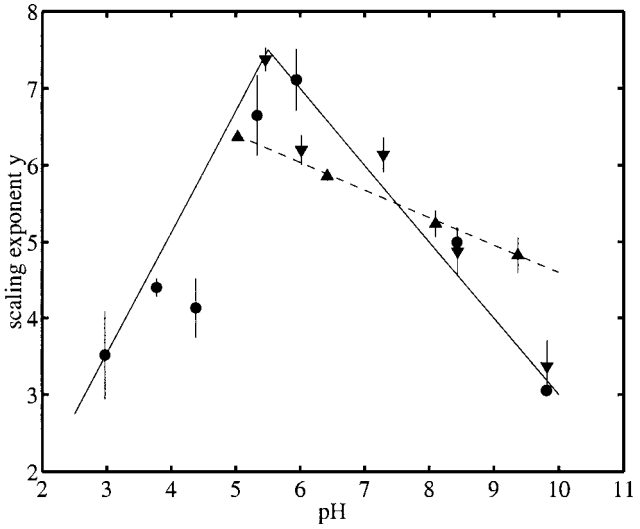

FIG. 5. Scaling exponent y as a function of *p*H, for buffers with different ionic strengths: (▲) $0.5<I<1.1$; (●) $0.008<I<0.012$; (▼) $0.001<I<0.003$. Continuous lines are a guide to the eye for low salt concentration behavior, the dashed line for high salt.

electric *p*H to 72 Å for high *p*H (due to the uncertainty in the spreading procedure the confidence in this result is ±10%).

Figure 4 shows a comparison of Π–Γ isotherms obtained using Wilhelmy plate methods and surface quasielastic light scattering. The error bars shown for the SQELS data are the error in the mean for fitting groups of five correlation functions as described above. At low surface concentrations there is good agreement between the static and dynamic measurements. However, at higher surface concentrations the value of the surface pressure measured using SQELS lies around 2×10^{-3} N/m above the static value. This discrepancy is considerably larger than the uncertainty in the fitting of the surface pressure. The onset of the deviation always occurs close to the maximum in the dilational modulus, as discussed below.

B. Scaling exponent and the semidilute regime

Figure 5 shows the variation of the pressure–concentration scaling exponent, y, as a function of *p*H. Data from experiments with three different ionic strengths (I) are included in this figure. It can be seen that the scaling exponent has a maximum at the isoelectric point, this indicates that the protein is most compact at this point. The peak value suggests that β-casein is close to θ condition and agrees with very recent work on the conformation of polyampholytes.[6] As the *p*H is varied away from the isoelectric point the exponent decreases, approximately linearly with the *p*H. This change in the exponent corresponds to a swelling of the polypeptide. The decrease in y is more dramatic at low I, indicating that screening charge interactions decreases the swelling effect of a net charge on the molecule. The exponent y changes more rapidly on the low *p*H side of the isoelectric point, as expected, since the calculated net charge changes more rapidly here than it does on the high *p*H side of the isoelectric point. Where indicated, error bars are the standard deviation of the mean of 2–8 repeated compressions, and they indicate the confidence to be expected for this kind of measure.

This behavior is in contrast to that observed in 3D polyampholyte gels, where there is a sharp step in the gel swelling as the overall charge is increased from neutrality through the threshold charge of $eN^{1/2}$. Here we see a more gradual change in the degree of swelling. In our system this critical value of net charge is anticipated to be $\approx 3e$. This degree of charging is achieved at a *p*H very close to the isoelectric point, therefore it is possible that the highly collapsed state has been missed. Also, the lower dimension of the surface layer compared to the bulk gel may play a part in changing the nature of the transition from collapsed to swollen states. This dimensional effect has been recently addressed in a Monte Carlo simulation of a diblock polyampholyte,[40] where it is argued that topological constraints modify the 3D coil–globule transition into a folding in 2D.

Figure 6 shows the variation of the scaling exponent with ionic strength for three ranges of *p*H.

For *p*H5–6, the scaling exponent decreases slightly with increasing ionic strength, corresponding to a small swelling of the protein. This behavior is consistent with that of a polyampholyte, where the screening out of opposite charge interactions will lead to chain expansion. An alternative explanation for this small effect is that increased ionic strength facilitates a small increase in overall charge leading to an overall chain expansion due to the increased importance of like charge repulsions.

The exponent y is constant with I for *p*H7.5–8.5, meaning that the polyampholyte tendency to contract is balanced by the net charge present on the molecule at that *p*H.

For *p*H9–10, the scaling exponent varies considerably with ionic strength. It exhibits a minimum at around $I=0.003$ M, i.e., below this value of I it decreases with increasing ionic strength and above it it increases. This mini-

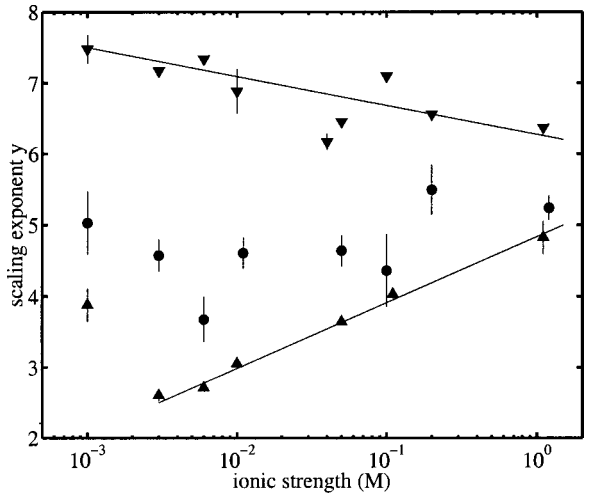

FIG. 6. Scaling exponent y as a function of ionic strength, for buffers with different pH: (▲) $9<p\mathrm{H}<10$; (●) $7.5<p\mathrm{H}<8.5$; (▼) $5<p\mathrm{H}<6$. Lines are a guide to the eye.

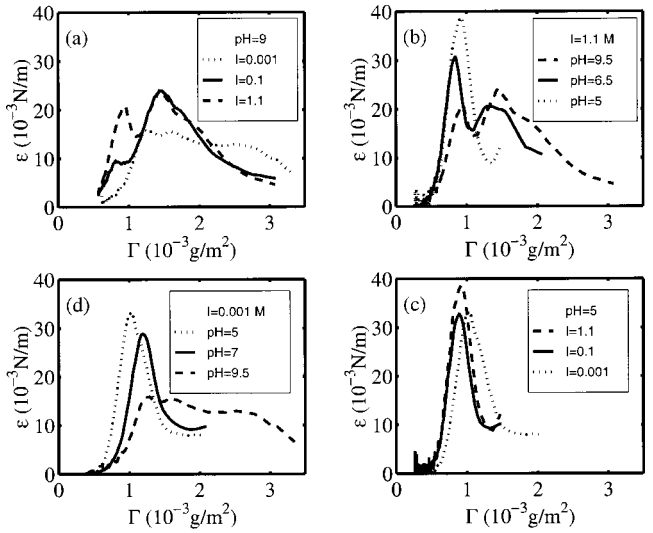

FIG. 7. Dilational modulus ϵ_{st} obtained from surface pressure isotherms over a range of subphase conditions. (a) and (c) show the effect of varying the ionic strength I at fixed pH, (b) and (d) the effect of varying pH at fixed I.

mum in the scaling exponent corresponds to a maximum in the chain swelling, and the nonmonotonic behavior would appear consistent with polyampholyte behavior at low ionic strength followed by polyelectrolyte behavior at higher ionic strength. This conclusion is probably incorrect though, because at the same ionic strength as the minimum in the scaling exponent ($I=0.003$ M) we find gross changes in the dilational modulus isotherms. Above this ionic strength there are two peaks in the dilational modulus and below there is only one. As discussed in detail below, these features probably correspond to gross changes in the surface configuration of the protein, with parts of the molecule moving into the subphase. It is therefore possible that the minimum in the scaling exponent arises from this gross structural change rather than a change in behavior of an essentially homogenous series of protein configurations. The distribution of positive and negative charges in β-casein is nonrandom, it may be that some of the features seen are due to this nonrandomness. Theoretical work[41] suggests that correlations in the sequence of positive and negative charges are important when the correlation length is of a similar size to the estimated charged blob. For the opposite extreme, where the charge sign alternates, the effect is unimportant. The value of the scaling exponent at high pH and low salt is in fair agreement with the prediction that a polyelectrolyte will behave as an extended chain.[6,42]

Our experimental results can also be compared to previous results on the swelling of 3D polyampholyte gels as a function of ionic strength, where nonmonotonic swelling behavior has been observed as a function of ionic strength. English *et al.*[10] found a maximum in gel swelling, Nisato *et al.*[9] see only a minimum in swelling as a function of increasing ionic strength.

C. Dilational modulus: $\epsilon-\Gamma$ isotherms

The scaling exponents in the previous section probe the proteins when they have just started to come into contact with one another. We will now use the dilational modulus (ϵ) to probe the behavior as the protein is further compressed. Dilational moduli–surface concentration plots for a range of pH and ionic strength are shown in Figure 7. Each figure contains data where one of pH and ionic strength is held constant whilst the other is varied. (a) Shows data for fixed $p\mathrm{H}=9.5$ and ionic strength varying from 0.001 to 1.1, here two peaks are seen in ϵ, one at around $\Gamma=0.8\times10^{-3}$ g/m^2 and the other at around 1.5×10^{-3} g/m^2, the magnitude of both of these two peaks increases as a function of increasing ionic strength. At the lowest ionic strength the peak at lower Γ is not apparent. (b) Shows data for fixed ionic strength=1.1 and pH varying from 5 to 9.5. Once again two peaks are observed in the dilational modulus at $\Gamma=0.8$ and 1.5×10^{-3} g/m^2, although they shift to slightly higher Γ as pH is reduced. In contrast to the data in (a), the magnitude of the peak at $\Gamma=0.8$ increases with reducing pH but that at higher Γ decreases in magnitude. (c) Shows data for fixed $p\mathrm{H}=5.0$ and ionic strength varying between 0.001 and 1.1, here only a single peak in the dilational modulus is observed which shifts to slightly higher Γ as ionic strength is reduced and shows little change in magnitude. Finally, (d) shows data at fixed ionic strength=0.001 and pH varying from 5 to 9.5 once again only one peak in the dilational modulus is observed, this shifts to higher Γ with increasing pH and reduces in intensity.

Note that increasing ionic strength corresponds to reducing the electrostatic screening length from 96 Å to 3 Å. Increasing pH above 5 leads to increased overall charge on the protein.

Previously, for β-casein, only a single peak in the dilational modulus at lower Γ has been commented upon, being attributed either to the collapse of the N-terminal end of the protein into the subphase,[22] or to looping of parts of the molecule in the subphase.[30] We propose that the first peak corresponds to the tail collapse in the subphase, and that the second peak arises from the collapse of a second region of the molecule into the subphase, this may well be the loop

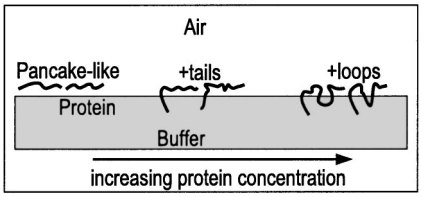

FIG. 8. Schematic diagram of the β-casein molecule at the air/buffer interface. At low concentration Γ the molecule lies on the surface with a ''pancake'' configuration. As Γ increases, first tails then loops of molecule are forced into the subphase.

region identified by examination of the primary sequence discussed above. These transitions that depend on concentration, *p*H and *I* are illustrated schematically in Fig. 8.

To our knowledge no synthetic system, even a multiblock copolymer, has been shown to exhibit two maxima in the dilational modulus as a function of surface concentration.

D. Dilational modulus: Surface transitions

We have further analyzed these data by observing the pressures where maxima and minima in the dilational modulus occur, as a function of *p*H and ionic strength (*I*). By considering a maximum in ϵ as the onset of a conformation transition and the successive minimum as the end of the transition, we are in the position to present ''configuration maps'' of the protein monolayer.

In Fig. 9 we show the effect of ionic strength. Shaded regions are for surface concentrations where ϵ is decreasing, these are the regions in which transitions between configurations occur. The transition corresponding to the first peak in ϵ is labeled as t_A (we are proposing that this is the tail protruding in the subphase), and the transition corresponding to the second peak is t_B (this would be the looping of some segments). The most obvious effect of salt addition is to move all transitions to higher Π. This means that transitions become more energetically costly the more charge interactions are screened. From Fig. 9 it is now clear how a two peak structure turns into a single peak for very low *I*. At the isoelectric *p*H, Fig. 9(a), one sees that the transition t_A does not occur at low *I*. This is consistent with the picture that a neutral polyampholyte is compact and tightly folded. Thus there no tail can easily be submerged. On the contrary at the other limit of high *p*H in Fig. 9(c), the tail transition t_A appears well defined and at low *I* it disappears at $\Pi=0$, meaning that the tail is already submerged at $\Gamma=\Gamma^*$ when the polymers first come into contact.

In Fig. 10 we show the effect of *p*H. The general feature is that as the *p*H increases and the molecule develops a net charge, all transitions occur at lower surface pressure.

In Fig. 10(a), low *I*, one sees that the tail transition t_A is not resolved from t_B at *p*H5, and emerges from *p*H around 7.5. It is very thin, meaning that the energy difference between conformations with the tail submerged or on the surface is very small. Also it appears that t_A is moving to $\Pi=0$, thus confirming that at high *p*H and low *I* we expect the tail to be spontaneously submerged.

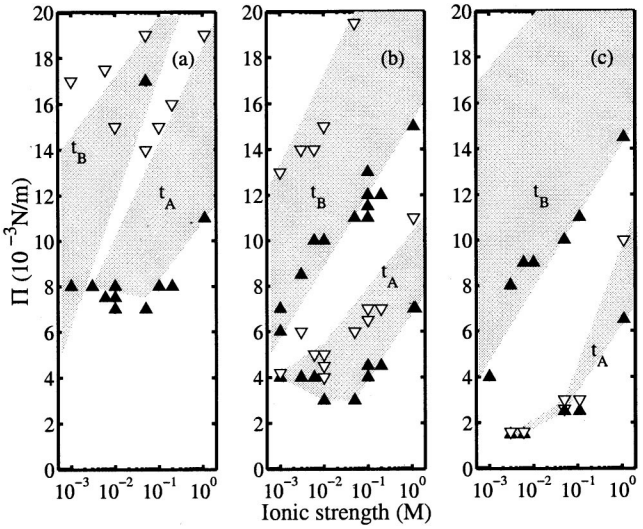

FIG. 9. ''Configuration maps'' at fixed *p*H and varying *I*, obtained from ϵ_{st}–Π isotherms. (▲) are the location of maxima in ϵ_{st}–Π plots and (▽) correspond to minima. Shaded areas, labeled t_A and t_B, guide the eye to regions of decreasing ϵ with increasing Π. We tentatively associate t_A as the region where the molecule forms tails in the subphase, and t_B as where it additionally forms loops. (a) $5<p\mathrm{H}<6$; (b) $7.5<p\mathrm{H}<8.5$; (c) $9<p\mathrm{H}<10$.

Moving to Figs. 10(b) and 10(c) one sees that t_A broadens with increasing *I*, and the loop transition t_B shifts towards the upper Π limit of our study.

We note that previous studies[30] have shown the β-casein monolayer to wholly collapse into a multilayer at pressures around 22×10^{-3} N/m, so for $\Pi\geqslant20\times10^{-3}$ N/m it would not be very significant to explain ϵ behavior in terms of single molecule conformation.

The concentrations at which the peaks in the dilational modulus occur are consistent with the calculated area cov-

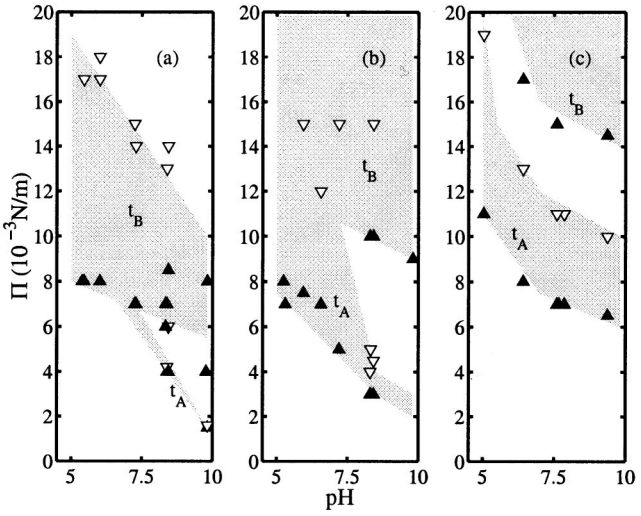

FIG. 10. ''Configuration maps'' at fixed *I* and varying *p*H, obtained from ϵ_{st}–Π isotherms. (▲) are the location of maxima in ϵ_{st}–Π plots and (▽) correspond to minima. Shaded areas, labeled t_A and t_B, guide the eye to regions corresponding to a decreasing ϵ with increasing Π. We tentatively associate t_A as the region where the molecule forms tails in the subphase, and t_B as where it additionally forms loops. (a) $0.001<I<0.003$; (b) $0.008<I<0.012$; (c) $0.5<I<1.1$.

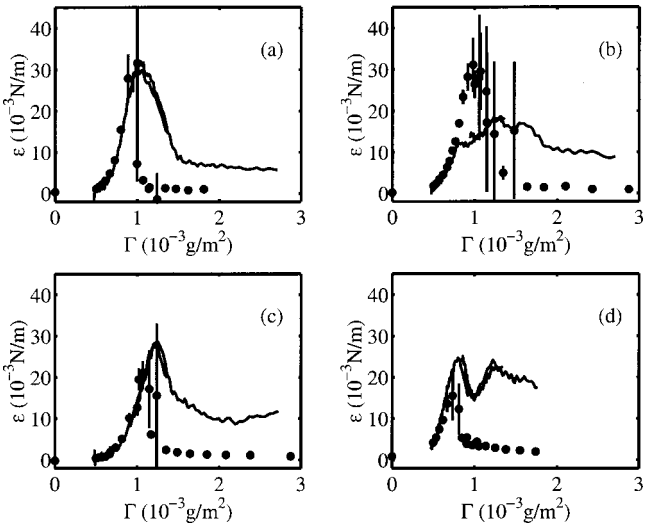

FIG. 11. Comparison of ''static'' ϵ–Γ isotherms (solid line) to dilational moduli obtained from surface light scattering for different subphase conditions (points): (a) *p*H=5.24, $I=0.01$; (b) *p*H=8.30, $I=0.01$; (c) *p*H=8.34, $I=0.001$; (d) *p*H=7.60, $I=1.1$.

ered by the protein with, successively, a terminal tail and a loop in the subphase. The peaks shift to lower concentrations with increased *p*H, this is consistent with the protein extending as more groups dissociate. The lower concentration peak reduces in magnitude as *p*H increases, whilst the higher concentration peak increases in magnitude with increasing *p*H. This is not unexpected, the free energy cost of forcing a longer loop into the subphase increases with loop length, since the ends of the loop must be constrained to the interface. The entropic cost of tail submersion depends less on length, as only one end is held at the surface.

E. Dilational modulus: High frequency

Figure 11 shows dilational moduli, obtained using SQELS as a function of surface concentration, compared with the values obtained from the static Π–Γ isotherm. At low surface concentration the static and dynamic values of ϵ are very similar, in common with the surface pressure measurements. At higher surface concentrations the dynamic, ϵ, value lies considerably below the static value. Once again the divergence of static and dynamic results occurs at or shortly before the first major maximum in the dilational modulus. The dynamic value of the dilational modulus only ever contains one strong maximum, unlike the static value which sometimes exhibits a peak at higher surface concentration. The significantly reduced value of the dynamic dilational modulus as compared to the static value has often been observed with soluble surfactants.[16] In these systems the difference arises from diffusion of surfactant out of the surface layer during the period of the dilational waves at the surface. This has been described theoretically by Lucassen *et al.*[43] and Hennenberg *et al.*[44] Here we do not anticipate a gross diffusional motion of the protein into and out of the surface layer at such high surface concentrations. However, it is probable that the motion of parts of the molecule into and out

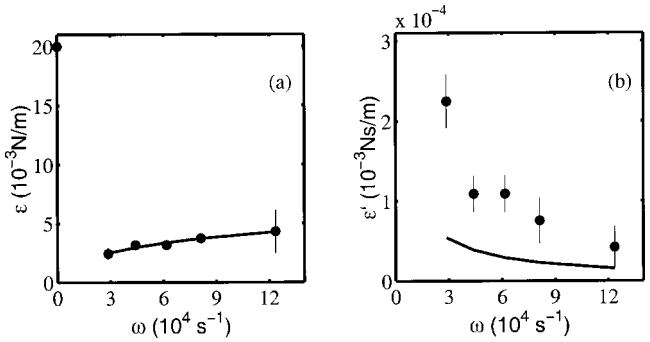

FIG. 12. Frequency dependence of the dilational modulus (a) and dilational viscosity (b) at *p*H=7.6, $I=1.1$, $\Pi=12\times10^{-3}$ N/m. This pressure is in the high concentration region, where the high frequency ϵ is consistently lower than the static ϵ_{st}. Solid lines both in (a) and (b) are the result of fitting the data in (a) with the model described by Eq. (11). In (a) the ϵ value plotted at $\omega=0$ is ϵ_{st} from the compression isotherm.

of the surface layer would have a similar signature.[45] Lucassen *et al.* find (here we use the notation of Langevin[16]),

$$\epsilon_0=\epsilon_{st}\left(\frac{1+\Omega}{1+2\Omega+2\Omega^2}\right)+i\epsilon_{st}\left(\frac{\Omega}{1+2\Omega+2\Omega^2}\right), \qquad (11)$$

where Ω is the reduced frequency,

$$\Omega=\sqrt{\frac{D}{2\omega}}\frac{dc}{d\Gamma}=\sqrt{\frac{1}{\omega\tau_c}}, \qquad (12)$$

where D is the diffusion coefficient of the surface species and c is the bulk concentration of adsorbant and thus τ_c is the characteristic time for this process of segment exchange between surface and subphase.

F. Dilational modulus: SQELS as a function of *q* at high surface concentration

By varying the scattering vector at which we collect SQELS data we vary the frequency, ω, of the capillary waves we observe. These data can then be tested against Eq. (11). This is done in Fig. 12. The data are in the high surface concentration regime where the static dilational modulus is larger than the SQELS modulus. A fit to the real part of the dilational modulus was made by varying the parameter τ_c and the static dilational modulus, ϵ_{st}. Fitted values are $\epsilon=9.2\times10^{-3}$ N/m and $\tau_c=12$ μs. The value of ϵ_{st} from the compression isotherm is 20×10^{-3} N/m. If we estimate the value of $dc/d\Gamma$ from data presented by Graham and Philips[20] the value of D obtained in this way is 7.5×10^{-11} m^2/s. The Lucassen model produces values of the dilational elasticity and viscosity of approximately the right magnitude, with the correct dependence on frequency, however, our data show a value of the complex part ($\omega\times\epsilon'$) which is larger than the real part (ϵ) and this cannot be accounted for by Eq. (11). The discrepancy may be due either to a systematic error in the determination of the dilational viscosity or to the fact that the type of behavior we anticipate is simply not modeled well by these expressions. Since the proposed mechanism is not simply diffusion into the bulk, the fitted values of τ_c might not have a real physical significance.

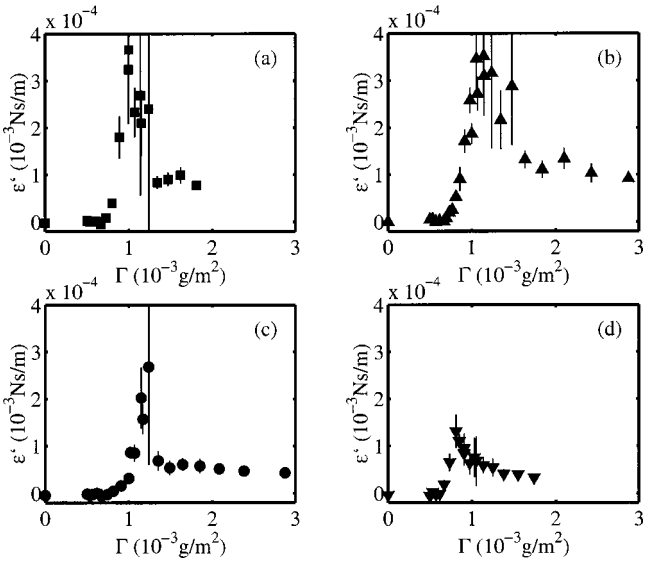

FIG. 13. Dilational viscosities obtained from surface light scattering for different subphase conditions: (a) pH=5.24, $I=0.01$; (b) pH=8.30, $I=0.01$; (c) pH=8.34, $I=0.001$; (d) pH=7.60, $I=1.1$.

Figure 13 shows values of the dilational viscosity obtained using SQELS. We have not measured low frequency values with which to compare this data. However, we find that the dilational viscosity of β-casein is very similar to that reported in the literature for other polymer monolayers measured by SQELS.[45] The dilational viscosity exhibits a maximum at the same surface concentration as the maximum in the dynamic dilational modulus.

G. SQELS as a function of q at low surface concentrations

In the previous section data from a range of q vectors (and thus frequencies) were introduced for layers at high surface concentrations. Here we consider similar data acquired at low surface concentrations. Figure 14 shows dilational modulus and viscosity as a function of q for a protein with surface concentration 0.8×10^{-3} g/m^2 on a buffer with pH=8.3 and $I=0.01$ M. This corresponds to a point close in concentration to the first peak in the dilational modulus, where the dynamic values of dilational modulus lie slightly above the static values [see Fig. 11(d)]. We fit these data using a Maxwell fluid model, i.e., a serial combination of a spring and dashpot, characterized by a single relaxation time, τ_m. The complex dilational modulus is given by

$$\epsilon_0=\left(\epsilon_{\rm st}+\epsilon_\infty\frac{(\omega\tau_D)^2}{1+(\omega\tau_D)^2}\right)+i\left(\epsilon_\infty\frac{\omega\tau_D}{1+(\omega\tau_D)^2}\right), \qquad (13)$$

where the first term is the dilational (elastic) modulus and the second part is the dilational viscosity. $\epsilon_{\rm st}$ is the static dilational modulus, ϵ_∞ is the amplitude of the relaxation, and ω is the frequency of measurement. The fit to the data is shown by a solid line, a single relaxation time of 23 μs. We believe that this relaxation time is related to a tail submersion event during the period of the dilational wave. It only appears strongly at high pH and moderately low I, that is, as discussed above [see Figs. 9 and 10], the conditions where the energy difference between absorbing and desorbing the tail is small. Assuming, as we have found, that an expression such as Eq. (13) holds, then the relaxation time τ_D can be obtained from the static dilational modulus and the dynamic dilational modulus and viscosity measured at a single frequency,

$$\tau_D=\frac{\epsilon_0-\epsilon_{\rm st}}{\omega\epsilon'}. \qquad (14)$$

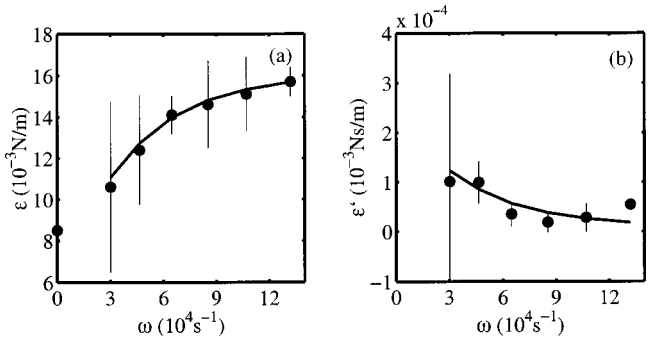

FIG. 14. Frequency dependence of the dilational modulus (a) and dilational viscosity (b) at pH=8.3, $I=0.01$, $\Pi=2\times10^{-3}$ N/m. This pressure is close to the first conformation transition region, where, for some subphase conditions, we observe a high frequency ϵ bigger than the static $\epsilon_{\rm st}$. Solid lines are best fits with the model described by Eq. (13). In (a) the ϵ value plotted at $\omega=0$ is $\epsilon_{\rm st}$ from the compression isotherm.

The results of this analysis (data not shown) are consistent with the more complete frequency measurements. Such relaxation times have been measured using SQELS by a number of groups for a number of polymer systems. Monroy *et al.*[46] found an Arrhenius temperature of the relaxation time for polyvinylacetate (PVAc) ($M_w=90\,000$), at the overlap concentration Γ^*. The relaxation time decreased from 80 μs at 1 °C to 5 μs at 25 °C. Monroy also finds relaxation times for mixed monolayers of PVAc and poly(4-hydroxystyrene) (P4HS).[45] The relaxation times are shorter for higher surface coverages and for larger fractions of the PVAc. Brown *et al.*[47] find relaxation times of this magnitude which reduce as a function of increasing surface concentration for polymethylmethacyrlate-poly-4-vinyl pyridine diblock copolymers. Richards *et al.*[48] find decreasing values of the relaxation time at lower concentrations, for PMMA-polyethylene oxide diblock copolymers, but at higher concentrations the relaxation times increase with increasing concentration. Mizuno *et al.*[49] also find a Maxwell relaxation, and they note that its physical origin can be a potential barrier to desorption.

H. Pressure relaxation data

We have carried out ''step compressions,'' where the surface layer is compressed at a constant rate for a short time and the evolution of the pressure (Π) is then measured for about 15 min, following which the next compression is performed. Similar measurements on other systems are reported for example by Monroy *et al.*[50] Such measurements have an obvious parallel with step strain measurements made on bulk materials.

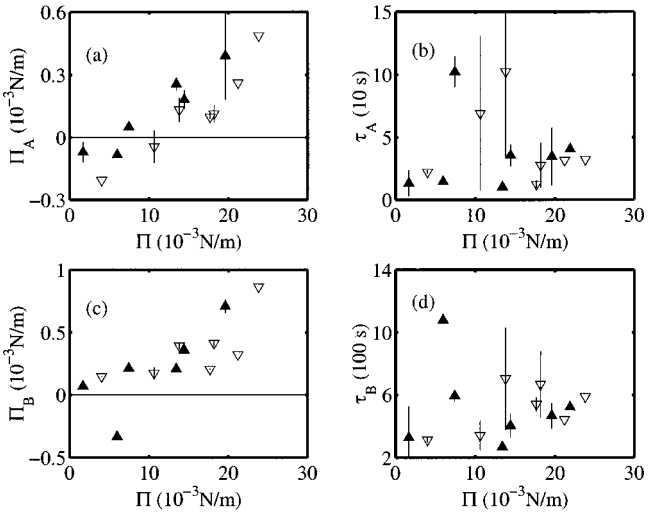

FIG. 15. Parameters describing the relaxation of pressure after a ''step-compression,'' fitted with the form shown in Eq. (15). (▲) correspond to a buffer *p*H=5.60, $I=0.1$ and (▽) to *p*H=8.32, $I=0.01$.

We find that a single exponential decay is insufficient to fully describe the data (this was also observed in Ref. 30 at high Π), but that in every case the spectra can be fitted with a sum of two exponentials with well separated time constants,

$$\Pi(t)=\Pi_A e^{-t/\tau_A}+\Pi_B e^{-t/\tau_B}+\Pi_C, \tag{15}$$

where Π_A and Π_B are the amplitudes of relaxations with time constants τ_A and τ_B. We find that the fast mode time scale is $20<\tau_A/s<50$ and the slow mode time scale is $300<\tau_B/s<700$. Π_C is a constant pressure offset (the equilibrium pressure) and t is the time since the end of the last constant rate compression. Figure 15 shows fitted values for these parameters from two sets of step compressions, measured on buffers at the isoelectric *p*H with $I=0.1$ and at *p*H=8.3 with $I=0.01$. These buffer conditions are chosen because they correspond to very different isotherms. The ratio between successive areas is always $\Delta A/A=0.55$. We are exploring a more complete range of subphase conditions and we refer to a future work for a complete presentation of these results.[50]

Figures 15(a) and 15(c) show the amplitudes Π_A and Π_B, respectively, of the fast and slow relaxations, as a function of the equilibrium pressure Π_C. One sees a general trend for the relaxations to become bigger as the pressure increases. At low Π negative values of both Π_A and Π_B are sometimes found. These are puzzling, as a negative amplitude reflects the fact that the pressure increases after the compression has ended. Although the data presented is too limited to support a strong conclusion, we observe that negative amplitudes for the slow mode (Π_B) occur only for buffer conditions that present a ''tail submersion'' transition, and then only around the transition pressure.

We believe that the fast mode is connected to relaxation of stress in the direction parallel to the compression, and that the slow mode is connected to stress relaxation between the parallel and normal directions. These stresses arise because the fast step compression induces a concentration gradient parallel to the compression, and can also bring the monolayer to a transient state where the strain in the direction of compression is greater than in the normal direction. We further suggest that below the ''loop transition'' pressure (which is in most conditions around $\Pi=10\times10^{-3}$ N/m, see Fig. 10) the surface pressure relaxations can be understood on the basis of the concavity of the equilibrium Π–Γ isotherm. On the contrary, above the loop transition, a fast compression does not give time to the monolayer to equilibrate with the subphase, and thus one cannot refer to the equilibrium isotherm.

In Figs. 15(b) and 15(d) we show the time scales τ_A and τ_B, respectively, of the fast and slow relaxations, as a function of the equilibrium pressure Π_C.

Noskov[51] has modeled these relaxations, and his work is relevant to understanding the observed relaxation time scales. He describes the interfacial relaxations as analogous to the Rouse-type relaxation modes of a bulk gel and how the presence of loops and tails of the polymer in the subphase leads to some degree of entanglement.

IV. CONCLUSIONS

We have measured the interfacial behavior of β-casein as a function of *p*H and ionic strength with high frequency light scattering and conventional methods. We find scaling exponents in the ''semidilute'' regime that agree with calculations reported in the literature for either polyampholytes or polyelectrolytes, depending on the charge present on the protein. In particular, we find that close to overall neutrality the protein molecule behaves like a random walk; as the *p*H is moved from the isoelectric *p*H the protein expands continuously almost reaching an extended chain configuration. At high *p*H and very low salt concentration, where the protein is overall negative, we observe an effective swelling then deswelling of the chain as a function of increasing ionic strength. At higher ionic strength the chain acts like a polyelectrolyte. Here only short range interactions are possible and, since the chain is overall charged, these interactions will be predominantly repulsive, weakening as the screening length is further reduced thus leading to deswelling of the chain.

Interfacial relaxation times have also been measured using both surface quasielastic light scattering and strain relaxation measurements. These suggest that at low surface concentrations the proteins act like independent disks, whilst at higher surface concentrations the layer forms an entangled network with Rouse-type relaxation modes.

The dilational modulus exhibits one or two peaks as a function of surface concentration, depending on the buffer conditions. These peaks are associated with the collapse of hydrophilic parts of the molecule into the subphase and we present a ''configuration map'' showing the dependence of these surface transitions on *p*H and ionic strength. We suggest, tentatively, that the peak at lower concentrations corresponds to the penetration of a tail from one end of the molecule and that at the higher concentration is associated with a loop. This conclusion is supported by the discovery of prospective loop and tail regions in the amino acid sequence of

the protein, whose sizes broadly match the positions at which the peaks occur in the dilational modulus.

β-casein was chosen, in part, because as a random coil protein it should most resemble a synthetic or model polyampholyte. We believe this is the first such study of this type, in applying ideas relating to polyampholytes to the understanding of proteins at interfaces. We are currently conducting a similar study into the behavior of a globular protein, to compare with our results from β-casein. We expect the degree of similarity to the observed behavior of β-casein to depend on the extent to which the globular protein unfolds at the surface.

ACKNOWLEDGMENTS

We are grateful to Unilever Plc and EPSRC for funding and to Professor Randal Richards and Dr. Mark Taylor for advice and encouragement regarding the design and construction of the SQELS apparatus. We would also like to thank Dr. Peter Wilde, Dr. Martin Buzza, and Peter Bermel for useful discussions.

[1] S. E. Kudaibergenov, Adv. Polym. Sci. **144**, 120 (1999).
[2] P. G. Higgs and J.-F. Joanny, J. Chem. Phys. **94**, 1543 (1991).
[3] N. Lee and D. Thirumalai, J. Chem. Phys. **113**, 5126 (2000).
[4] Y. Kantor and M. Kardar, Phys. Rev. E **51**, 1299 (1995).
[5] N. Lee and S. Obukhov, Eur. Phys. J. B **1**, 371 (1998).
[6] V. Yamakov, A. Milchev, H. J. Limbach, B. Dünweg, and R. Everaers, Phys. Rev. Lett. **85**, 4305 (2000).
[7] M. Tanaka and T. Tanaka, Phys. Rev. E **62**, 3803 (2000).
[8] A. V. Dobrynin and M. Rubenstein, J. Phys. II **5**, 677 (1995).
[9] G. Nisato, J. P. Munch, and S. J. Candau, Langmuir **15**, 4236 (1999).
[10] A. E. English, S. Mafé, J. A. Manzanares, X. Yu, A. Y. Grosberg, and T. Tanaka, J. Chem. Phys. **104**, 8713 (1996).
[11] J.-M. Corpart and F. Candau, Macromolecules **26**, 1333 (1993).
[12] R. A. L. Jones and R. W. Richards, *Polymers at Surfaces and Interfaces* (Cambridge University Press, Cambridge, 1999).
[13] A. W. Adamson and A. P. Gast, *Physical Chemistry of Surfaces*, 6th ed. (Wiley, New York, 1997).
[14] D. Möbius and R. Miller, *Proteins at Liquid Interfaces* (Elsevier, Amsterdam, 1998).
[15] M. Daoud and G. Jannink, J. Phys. (Paris) **37**, 973 (1976).
[16] D. Langevin, *Light Scattering by Liquid Surfaces and Complementary Techniques* (Dekker, New York, 1992).
[17] A. Bairoch and R. Apweiler, Nucl. Acids Res. **28**, 45 (2000).
[18] H. E. Swaisgood, in *Developments in Dairy Chemistry*, edited by P. F. Fox (Applied Science Publishers, London, 1982), Vol. 1, pp. 1–59.
[19] E. Dickinson, D. S. Horne, J. S. Phipps, and R. M. Richardson, Langmuir **9**, 242 (1993).
[20] D. E. Graham and M. C. Philips, J. Colloid Interface Sci. **70**, 415 (1979).
[21] J. R. Hunter, P. K. Kilpatrick, and R. G. Carbonell, J. Colloid Interface Sci. **142**, 429 (1991).
[22] M. Mellema, D. C. Clark, F. A. Husband, and A. R. Mackie, Langmuir **14**, 1753 (1998).
[23] R. E. Anderson, V. S. Pande, and C. J. Radke, J. Chem. Phys. **112**, 9167 (2000).
[24] F. A. M. Leermakers, P. J. Atkinson, E. Dickinson, and D. S. Horne, J. Colloid Interface Sci. **178**, 681 (1996).
[25] R. Douillard, M. Daoud, J. Lefebvre, C. Minier, G. Lecannu, and J. Coutret, J. Colloid Interface Sci. **163**, 277 (1994).
[26] V. Aguié-Béghin, E. Leclerc, M. Daoud, and R. Douillard, J. Colloid Interface Sci. **214**, 143 (1999).
[27] V. B. Fainerman and R. Miller, Langmuir **15**, 1812 (1999).
[28] P. Calmettes, D. Durand, V. Receveur, M. Desmadril, P. Minard, and R. Douillard, Physica B **213**, 754 (1995).
[29] R. M. C. Dawson, D. C. Elliot, W. H. Elliot, and K. M. Jones, *Data for Biochemical Research* (Clarendon, Oxford, 1959).
[30] M. R. R. Niño, C. C. Sánchez, and J. N. R. Patino, Colloids Surf., B **12**, 161 (1999).
[31] J. C. Earnshaw and R. C. McGivern, J. Phys. D **20**, 82 (1987).
[32] S. Hård and R. D. Neuman, J. Colloid Interface Sci. **83**, 315 (1981).
[33] P. J. Winch and J. C. Earnshaw, J. Phys. E **21**, 287 (1988).
[34] F. C. Goodrich, Proc. R. Soc. London, Ser. A **374**, 341 (1981).
[35] M. Daoud and P. G. de Gennes, J. Phys. (Paris) **38**, 85 (1977).
[36] R. Vilanove and F. Rondelez, Phys. Rev. Lett. **45**, 1502 (1980).
[37] J. C. Earnshaw, R. C. McGivern, A. C. McLaughlin, and P. J. Winch, Langmuir **6**, 649 (1990).
[38] D. M. A. Buzza, J. L. Jones, T. C. B. McLeish, and R. W. Richards, J. Chem. Phys. **109**, 5008 (1998).
[39] J. C. Earnshaw and R. C. McGivern, J. Colloid Interface Sci. **123**, 36 (1988).
[40] J. B. Imbert, J. M. Victor, N. Tsunekawa, and Y. Hiwatari, Phys. Lett. A **258**, 92 (1999).
[41] P. G. Higgs and J. F. Joanny, J. Chem. Phys. **94**, 1543 (1991).
[42] J. F. Joanny, M. Castelnovo, and R. Netz, J. Phys.: Condens. Matter **12**, A1 (2000).
[43] J. Lucassen and M. v. d. Tempel, J. Colloid Interface Sci. **41**, 491 (1972).
[44] M. Hennenberg, X.-L. Chu, A. Sanfeld, and M. G. Verarde, J. Colloid Interface Sci. **150**, 7 (1992).
[45] F. Monroy, F. Ortega, and R. G. Rubio, J. Phys. Chem. B **103**, 2061 (1999).
[46] F. Monroy, F. Ortega, and R. G. Rubio, Phys. Rev. E **58**, 7629 (1998).
[47] A. S. Brown, R. W. Richards, D. M. A. Buzza, and T. C. B. McLeish, Faraday Discuss. **112**, 309 (1999).
[48] R. W. Richards, B. R. Rochford, and M. R. Taylor, Macromolecules **29**, 1980 (1996).
[49] D. Mizuno, K. Hattori, N. Sakamoto, K. Sakai, and K. Takagi, Langmuir **16**, 643 (2000).
[50] P. Cicuta and I. Hopkinson (in preparation).
[51] B. A. Noskov, Colloid Polym. Sci. **273**, 263 (1995).